Islamic Azad University
Mashhad Branch

*Eslamizadeh / Iranian Journal of Earth Sciences 8 (2016) / 147-163*

# Geological setting of iron oxide-apatite deposits in the Bafq district, central Iran with an emphasis on mineralogical, petrographic, and geochemical study of the Sechahun deposit

**Azat Eslamizadeh*[1]**

*1. Department of Geology, Bafgh Branch, Islamic Azad University, Bafgh Iran*

Received 2 October 2015; accepted 17 April 2016

## Abstract

The objective of this research is to determine all processes in the magmatic evolution and related hydrothermal activities that created the volcanic rocks and associated ore-forming systems of the Bafq mining district. Several iron oxide-apatite (IOA) deposits were investigated in this area with a focus on the Sechahun ore deposit. The Bafq mining district is well known for hosting significant IOA ore deposits with several million tons of iron ore and with some economic resources of rare earth elements. To achieve the goals of this research, detailed petrographic, fluid inclusion microthermometry, and lithogeochemical studies were obtained and supported by geological investigations at both local and regional scales. Textural, mineralogical, and fluid inclusion evidence indicates the ore genesis by fluid mixing. Magmatic-hydrothermal iron oxide-apatite ore precipitated during circulation of deuteric solutions within the host rocks at the early stage of mineralization. The mesothermal iron oxide ore of the Sechahun deposit was emplaced at the relatively shallow depths, while the near-surface epithermal hematite-jaspilite ore formed in a subaqueous environment. The most likely source of iron oxide-apatite mineralization would be a combined magmatic hydrothermal to convective hydrothermal model with magmatism originating from the upper mantle and related bimodal volcanism resulting in felsic volcanic rocks. Rifting of the continental lithosphere during the Early Cambrian was associated with emplacement of a highly fractionated bimodal magmas along the regional fracture-fault lines, a major controlling factor for mineralization processes in the Bafq district.

***Keywords:*** *iron oxide-apatite, petrography, geochemistry, Sechahun, Bafq*

## 1. Introduction

The Posht-e-Badam Block in Central-East Iranian microcontinent is known as the main metallogenic province of Iran, hosting many ore deposits particularly iron oxide-apatite (IOA), Fe-Mn exhalative, and Zn-Pb sedimentary exhalative types (Rajabi et al. 2015). Sechahun is one of the most important iron ore deposits among 34 magnetic anomalies of the Bafq mining district in the Posht-e-Badam Block.

The Bafq mining district, containing several million tons of iron ore and some economic REE resources, has good potential for further international studies regarding to metallogenesis of IOA and iron oxide-copper-gold (IOCG) ore deposits. The iron oxide ore deposits of the Bafq district are known as the Kiruna-type deposits due to the same age of formation as related volcanic and plutonic host rocks (Daliran 2002; Gandhi 2003; Daliran et al. 2009, 2010). According to U-Pb LA-ICP-MS age (Bonyadi et al. 2011), REE-rich fluorapatite from the Sechahun deposit formed at 510±8 Ma, at the end of the main regional sodic magmatism (525±7 Ma). Based on this age, the large-scale sodic alteration and magnetite-apatite mineralization occur in volcano-sedimentary sequence that are intruded by sodic granitoids. U-Pb dating was used by Stosch et al. (2011) for inclusion-free apatites in the Bafq area; it indicates an age range from 539 to 527 Ma, including U-Pb zircon ages (528±1 Ma). The Early Cambrian felsic volcanic host rocks had also been dated by Ramezani and Tucker (2003). U-Th-Pb dating of the monazite regularly preserved in the center of apatite crystals in the Choghart ore deposit indicates an age of 515±21 or 529±21 Ma (Torab and Lehmann 2007). Despite the numerous published reports, the age and origin of the iron oxide-apatite deposits of the Bafq mining district have remained uncertain and controversial. Based on Stosch et al. (2011), these Kiruna-type iron oxide-apatite deposits formed within the felsic volcanic tuffs and volcano-sedimentary sequences in the Early Cambrian.

Recently, the Kiruna-type deposits are generally referred to as IOA (Williams 2010), or P-rich iron oxide deposits (Groves et al. 2010). In addition to volcanic rocks, other hosts of the P-rich iron ore in the Sechahun area are limestone and dolomite. There are alternate layers of dolomite, hematite, and jaspilite in eastern highlands of the Sechahun area. According to Mohseni and Aftabi (2012), occurrence of these sedimentary rocks together with keratophyres, diamictites,

*Corresponding author.
*E-mail address (es):* meslamizadeh@bafgh-iau.ac.ir

dropstones, and phosphorous in the Sechahun area, have similarities with Rapitan-type banded iron-phosphorous formation rather than an incomplete IOCG ore model.

On the other hand, Bonyadi et al. (2011) showed convincingly that the Sechahun deposit is a member of the IOCG group, reiterating that evidence of IOCG affinities widely advanced for the Bafq mining district (Barton and Johnson 1996; Williams et al. 2005; Jami et al. 2007; Torab and Lehmann 2007; Daliran et al. 2010; Stosch et al. 2011) and the Sechahun deposit. This is based on magnetite- apatite mineralogy and related halos of high-temperature sodic-calcic alteration products that can be considered as an IOA member of the IOCG group. Hitzman (2000) redefined the IOCG class by dividing in two end-members, i.e., the Kiruna-type iron oxide-apatite deposits (IOA) and iron oxide-copper-gold (IOCG) types. Extensive research by Daliran (1990) and Daliran et al. (2009, 2010) shows that mineralization in the Sechahun IOA deposit occurred together with felsic magmatism of Early Cambrian age. Besides the felsic volcanic rocks, gabbro intrusions host the mineralization in some iron ore deposits of the Bafq district, such as Esfordi and Chagas (cf. Rajabi et al. 2015); in the Sechahun area as shown later in the petrographic description, there are many diabasic dykes intersecting the volcanic rocks. As mentioned by Daliran et al. (2009), this diversity of mineralization types is a result of the multi-stage hydrothermal–magmatic processes and a rift-related volcanic activity implied a temporal relationship between the magmatic system and ore-forming processes. Rajabi et al. (2015) suggested that both IOA and apatite-rich deposits in Central Iran are epigenetic and occurred within the syn-rift sequence of the Early Cambrian volcano-sedimentary sequence (ECVSS). Occurrences of some stratiform and stratabound ore bodies in this area suggests these deposits formed by sedimentary-exhalative activities shortly after the sedimentation. This theory supports a direct genetic relation between the iron-oxide apatite deposits, magmatic anomalies, and hydrothermal overprints. Based on this opinion, magmatic differentiation is the most reliable source of iron in this district. Hydrothermal alteration patterns and associated mineral assemblages are concluded with overviews on the use of geochemistry and petrography. The fluid inclusions in the Sechahun deposit are studied with the aim of identification and separate regional metasomatism from hydrothermal circulation. It is followed by further discussion about the magmatic differentiation processes and hydrothermal overprint. This study concludes that both magmatic (as direct crystallization in a liquid solution) and hydrothermal processes had a role in ore formation in the area.

## 2. Geological setting

The Bafq mining district is located in the middle of Kashmar-Kerman volcano-plutonic arc, between Kuhbanan and Kuhe-Daviran major fault structures of Central Iran. This magmatic arc hosts important Kiruna-type magnetite-apatite deposits and stretches as a narrow rift zone from Robat-Posht-Badam in the north to Bafq in the south (Stosch et al. 2011). Ramezani and Tucker (2003) suggested that the Kashmar-Kerman volcano-plutonic arc represented an active continental-margin environment in relation to subduction under the Central Iranian micro-plate and closure of the Proto-Tethys ocean in the Early Cambrian.

Rajabi et al. (2015) explained that the Posht-e-Badam Block in the Central Iranian micro-continent broke up during the Late Neoproterozoic-Early Cambrian continental back-arc rifting, parallel to convergence (Proto-Tethyan) along the continental margin (Berberian and King 1981; Hushmandzadeh 1989; Samani 1998a; Daliran 1990; Talbot and Alavi 1996; Rajabi et al. 2015).

Other researchers believe that the evolution followed major rifting stages. The first stage, syn-rift phase related to intra-basin extension, indicated by coarse-grained detrital sedimentary rocks and bimodal volcanism. Stage II involved the deposition of calcareous shale, siltstone, and carbonates. During this phase, sedimentation processes were controlled by basin subsidence and reactivation of the half-graben faults. It is believed that the magma erupted through a shallow marine environment, while sediments had not consolidated completely. As a result, a complex of sedimentary units together with altered vitric tuffs and volcanic rocks were created (Hushmandzadeh 1989). Finally, two types of uppermost Precambrian rock units, including riftogenic series and platform-type, cropped out in the region (Samani 1998b). There are two distinct parts known as Anomalies X and XI at the Sechahun mine (Fig 1). The Cambrian-Tertiary platform covered by limestone, dolomite, conglomerate, sandstone, and shale. The Precambrian basement in this area consists of schist, gneiss, marble, and quartzite. The igneous rocks with limited outcrops are granite, diorite, and gabbro-diorite. The Early Cambrian rocks containing iron-oxide apatite deposits are volcano-sedimentary sequences, mostly with alternation of rhyolite and dolomite (Fig 1).

## 3. Field investigation and Petrography

A wide complex of volcanogenic-sedimentary, metamorphic, and magmatic rocks participated in the geological structure of the Sechahun area. Based on geological mapping (Fig 1) and field investigation, there are three complexes of Precambrian-Early Cambrian, Cambrian-Tertiary, and Quaternary rocks in the area. The Precambrian formations occur chiefly in south of the Sechahun, northeast of the Bafq. They represent foundation protuberances composed of rhyolite, crystalline schist, gneiss, effusive green-rocks, and marble.

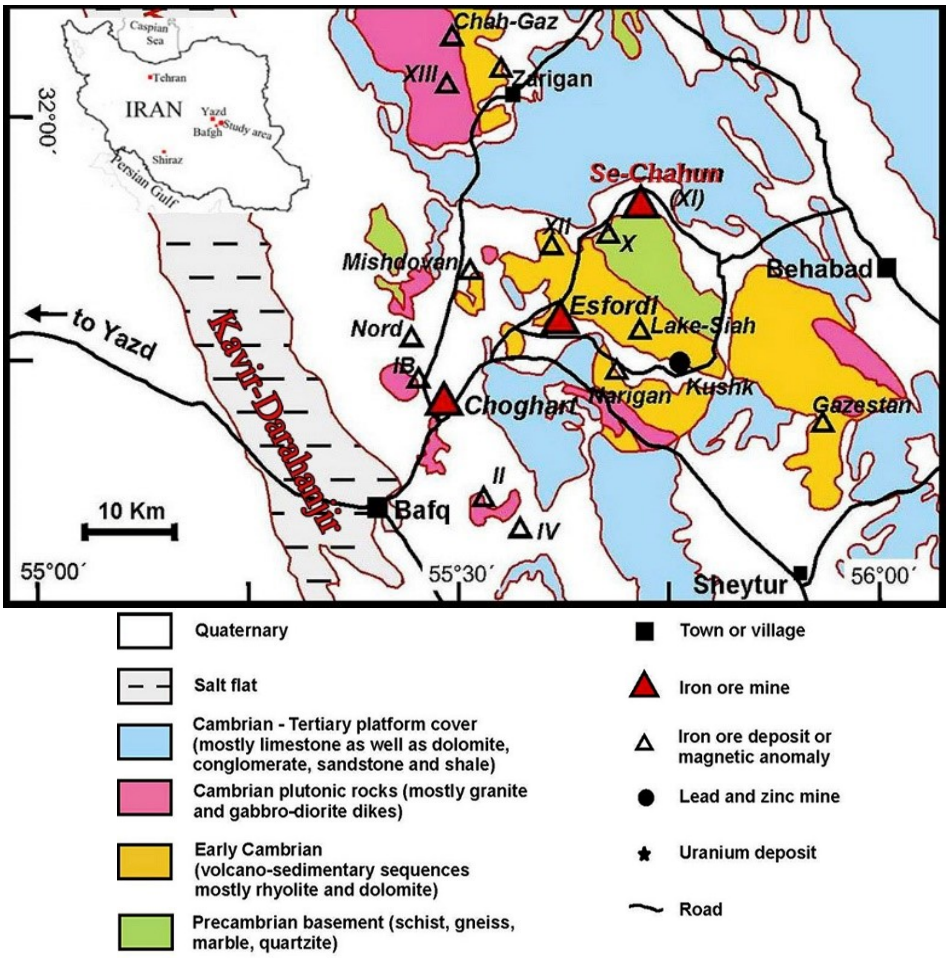


Fig 1. Geological map of the Bafq mining district (modified after Ramezani and Tucker 2003; Torab and Lehmann 2007). The IOA deposits of Sechahun, Choghart, Gazestan, Esfordi, and Chagas are shown in the map.

The Infracambrian volcano-sedimentary rocks singled out among the Precambrian formations. They are known as Rizu and Dezu series (Daliran 2002). The rocks of these series overlay the Precambrian units with a slightly significant unconformity. They include sandstone, schist (phyllite), limestone, dolomite, effusive with intercalations of conglomerate, tuff, and siliceous-ferruginous rocks. The main ore bodies consist of black massive magnetite. Brecciated textures resulted from changes in physical properties of the ore during sedimentation or later tectonic activity. Hydrothermally altered volcanic rocks known as the Green Rocks (Torab 2008; Eslamizadeh 2017) predominate especially along boundaries of the ore body (Fig 2).

The magnetite ore has frequently altered to hematite at the lower temperature conditions, and occurs as veins associated with effusive of acidic composition (altered tuffs), felsic volcanic rocks with intercalations of carbonaceous rocks, and green rocks (Fig 3a). Apatite is the main gangue mineral and widely scattered in magnetite ore bodies or seen as interfingering (Fig 3b). Apatite also crystallized forming granular textures. Silica-bearing magnetite with quartz veins occur in silicified zones (Fig 3c); this magnetite type is known as the low-grade ore. The carbonate rocks evidently developed in mineralized zones (Fig 3d).

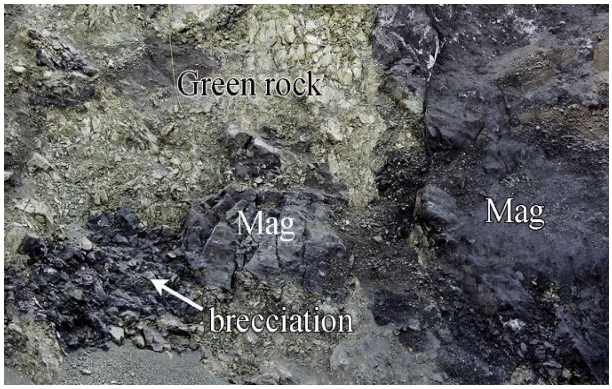


Fig 2. Green Rocks in contact with massive magnetite and brecciated zone.

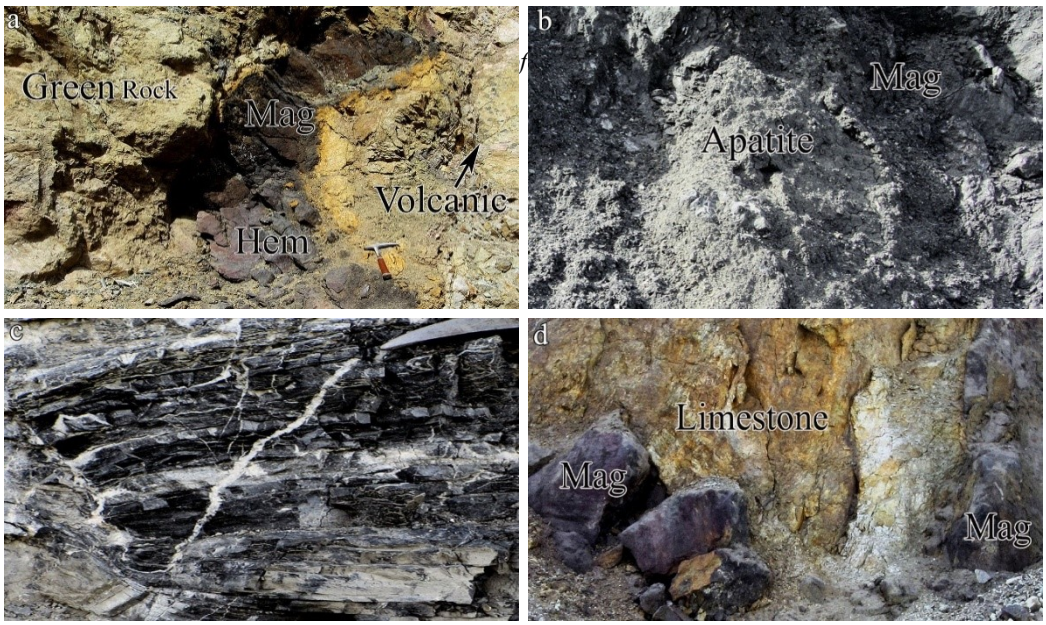


Fig 3. a. Magnetite-hematite vein in Green Rocks b. Interfingering growth of magnetite and apatite c. Silica-bearing magnetite d. Development of carbonate rocks in the mineralization area. Abbreviations as in table 1.

Table 1. The photomicrograph's abbreviations, based on Siivola and Schmid (2007).

| | | | | | |
|---|---|---|---|---|---|
| **Pl** | plagioclase | **Zo** | zoisite | **Mc** | microcline |
| **Ep** | epidote | **Px** | Pyroxene | **Hem** | hematite |
| **Bi** | biotite | **Cal** | calcite | **Al** | albite |
| **Act** | actinolite | **Qtz** | quartz | **Ttn** | titanite |
| **Tr** | tremolite | **Chl** | chlorite | **Mag** | magnetite |
| **Afs** | alkali feldspar | **Mar** | martite | **Op** | opaque |

The presence of the calcite-magnetite ore proves this, although metasomatic processes obscured this composition. Mineralization generally occurs along cross-cutting faults on the flanks of an anticline structure in the Sechahun deposit. The young Quaternary deposits crop out by the boulder-pebbly polygenic formation that cemented by a loamy-sandy material, gypsum, salts, sand, sandy limestone, and conglomerate. Petrographic study of the surrounding rocks of the Sechahun ore deposit indicates a widespread complex of volcanogenic-sedimentary, metamorphic, and magmatic rocks.

The holocrystalline rhyolite, trachyandesite, and crystal tuffs are the most abundant Early Cambrian igneous rocks in the study area. The iron-oxide apatite ore is closely associated with these rocks, both spatially and temporally. Other petrologic features in this area are the low-grade metamorphic rocks (green rocks), carbonate, and sub-volcanic rocks as diabasic dykes that intruded into the older formations. The sill-shaped syenitic rocks have lower volume than the silicic volcanic rocks (rhyolite and rhyodacite). Photomicrographs of the altered diabasic dykes are shown in Fig 4a. Basic plagioclases and interstitial mafic minerals are mostly subophitically intergrown. They altered to epidote, zoisite, clinozoisite, calcite, sericite, and chlorite (Fig 4b). Mafic minerals are mainly represented by tremolite-actinolitic amphiboles. The relics of pyroxenes are commonly preserved. These minerals were mostly converted to amphibole, chlorite, and calcite (Fig 4c). The rocks with a syenitic composition have a medium-grained, granular and porphyritic texture. The chessboard albite is the main feldspar (55-60%) constituent (Fig 4d). The microscopic study of thin sections shows that most of the sills plotted in the ortho-syenites category and even can be considered as albitite or saturated sodic syenite (Daliran 1990). The $Na_2O$ amount, based on the XRF analysis, reach to 9.05 wt% in syenitic rocks (sample no. 17s in table 2).

The porphyritic acidic rocks are mainly composed of quartz, feldspars, and a felsite groundmass of all these minerals. The feldspar phenocrysts seems to react to new solutions and fluids; they occur as very fresh up to totally altered and pseudomorphous crystals (Fig 4e, f). The albite phenocrysts have chessboard twinning, and some of them show a rim of alkali feldspar interfingering with the albite core (Fig 5a, c). The newly formed albite and quartz resulted from albitization of the primary feldspars and devitrification of volcanic glass.

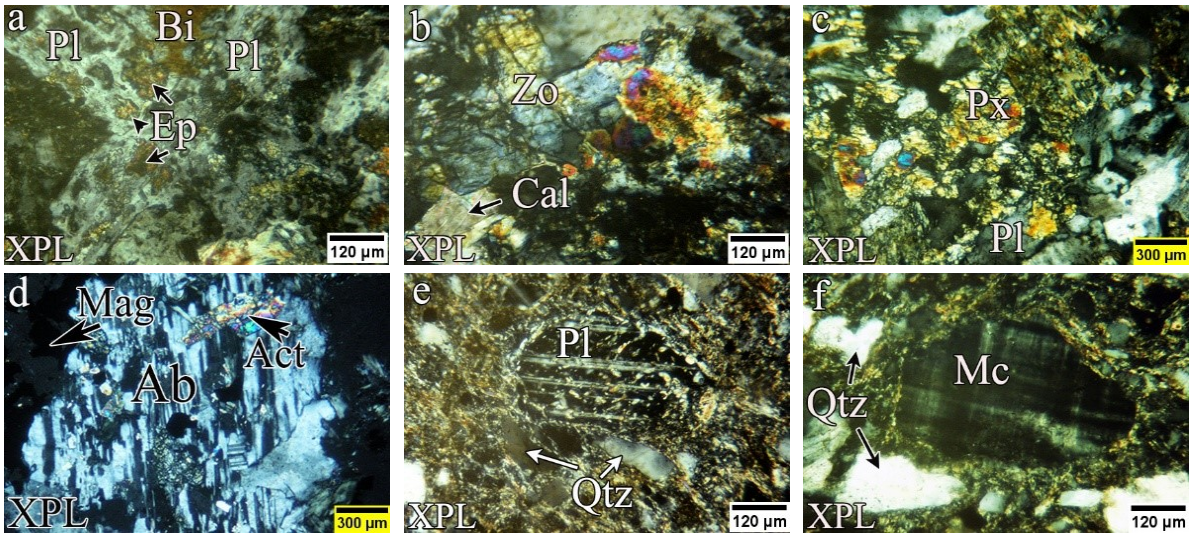


Fig 4. Photomicrographs (cross polarized light, XPL) of: a. Diabasic texture of dykes b. Zoisite/Clinozoisite c. The relic of pyroxene (diopside) d. Chessboard albite e. Sericitization of plagioclase f. Microcline

Replacement of Na for K in feldspars shown by the presence of albite inclusions in the K-feldspar host. Sodium migrates into the lattice as a distinct domain by creation of the perthitic texture. The structure can be turned back again to a K-rich domain in order to form microcline with further temperature decreasing (Pirajno 2009). All rock types in the Sechahun area display intensive and pervasive alteration. It seems that the final stage of hydrothermal activity had an important role in developing chemical alteration of rocks than earlier metasomatism in the Sechahun deposit. Sodic alteration is obvious from development of the chessboard texture and color changes due to K replacement by Na in perthite that leads to development of albitites. Albite, amphibole, epidote, hematite, and chlorite are the main mineral assemblage (Fig 5b). Creation of chessboard albite is an evidence for metasomatism in this area, but hydrolysis of silicate minerals and influence of hydrothermal fluids can be defined in volcanic rocks that resulted from a widespread alteration. Volcanic gases (HCl, $CO_2$, $H_2S$) could provide the $H^+$ ions and acted as the major acidifying factors during the processes of hydrothermal alteration (Pirajno 2009).

The volcanic rocks in the Sechahun deposit are related to potassic alteration and have a pinkish color that is mainly due to K-feldspar occurrence, containing fine-grained hematite inclusions (Fig 5d).

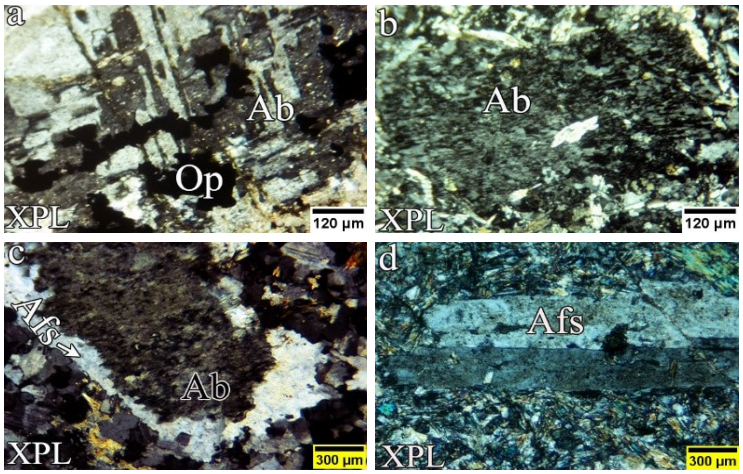


Fig 5. Photomicrographs in XPL of: a. Chessboard twinning of albite b. Chessboard albite in the sodic alteration zone c. Rim of alkali feldspar around albite d. Alkali feldspar (orthose) in the potassic zone

As noted by Pirajno (2009) after Kinnaird (1985) and Norberg et al. (2014), the reddish color of microclines in hand specimens occur due to Fe releasing in the primary feldspar structure during the K for Na exchange.

K-feldspar albitization was studied by Norberg et al. (2014) experimentally at 500°-750° C and 200 MPa. They showed that a portion of the K-feldspar was topotactically replaced by a highly complex polycrystalline and porous rim of high albite. Albitization of feldspars in the Sechahun deposits and some of the other deposits in the Bafq district, such as Mishdovan, North anomaly, and Zaghia (Eslamizadeh and Samanirad 2013), is commonly associated with releasing of Fe and REE. At the same time, there is evidence of silicification due to Si enrichment. Developing of albite domains and metasomatic K for Na exchange with development of microcline in the Sechahun sytem shown in Figs 4 and 5 by forming of chessboard albite and microcline neoformation. The stages summarized as schematic design based on Pirajno (2009) in Fig 6.

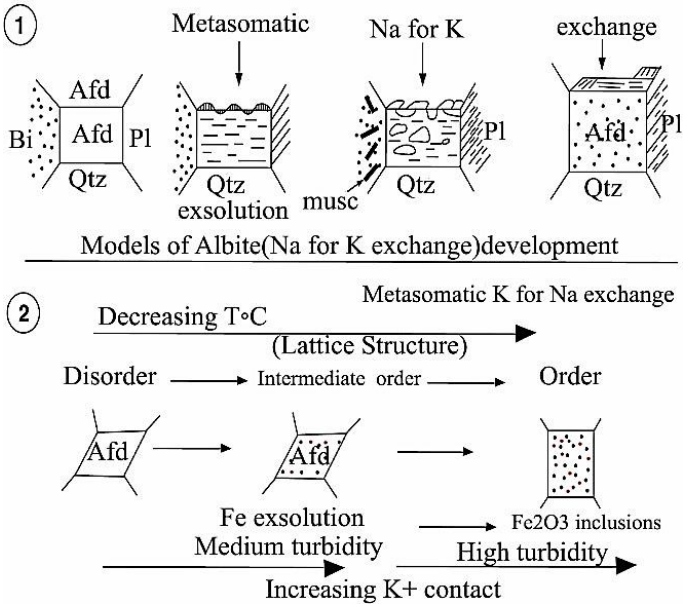


Fig 6. Metasomatism of alkali feldspar crystals. 1. Development of albite 2. Development of microcline (modified after Pirajno 2009)

The $^{40}Ar/^{39}Ar$ data on potassic alteration by Torab (2008) shows variably disturbed age spectra that reveal a younger thermal overprint at more than 300°C during the Mesozoic-Cenozoic evolution of Central Iran. Volcanic and subvolcanic host rocks in the Sechahun deposit have slightly changed during evolution by the sodic, potassic, and calcic overprints. These rocks have locally been brecciated. Fibrous amphibole, chlorite, epidote, and calcite are filled microfractures and open spaces between the crystals (Fig 7a, b, c). All these features prove that hydrothermal minerals precipitated during the late phases of hydrothermal activity.

Development of country rock actinolitization is common in the Bafq mining district. In the most deposits, such as Sechahun, Choghart, and Gazestan (Eslamizadeh and Samanirad 2016), the green rocks with a dark-green color consist of tabular needle-shaped tremolite and actinolite crystals, formed near the iron oxide veins. The crystals length occasionally extends up to 10 centimeters. In some iron ore deposits, such as Chador-Malu, formation of actinolite-rich metasomatic host rocks were considered by Sabet-Mobarhan-Talab et al. (2015) as an evidence of high-temperature fluids associated with hydrothermal mineralization. Actinolite also shows a dendritic intergrowth texture with magnetite (Fig 7d). The dendritic texture is common in the Kiruna-type iron ore deposits, and represented as one of the magmatic iron ore characteristics (Nystrom and Henriques 1994). Furthermore, there is an angle of 120° (foam-like) between the fine-grained magnetite grains in both the Sechahun (Fig 7e), and other Bafq iron ore deposits, like Zaghia (Eslamizadeh and Akbarian 2015), indicating the slow cooling rate and crystallization of magma (Förster and Jafarzadeh 1994). Magnetite grains in some cases display the ilmenite exsolution. Magmatic magnetite commonly develops oxy-exsolution of ilmenite (Liu et al. 2015). Also titanite occurs as a rim on magnetite along unbrecciated zones in Anomaly XI of Sechahun and Choghart (Fig 7f).

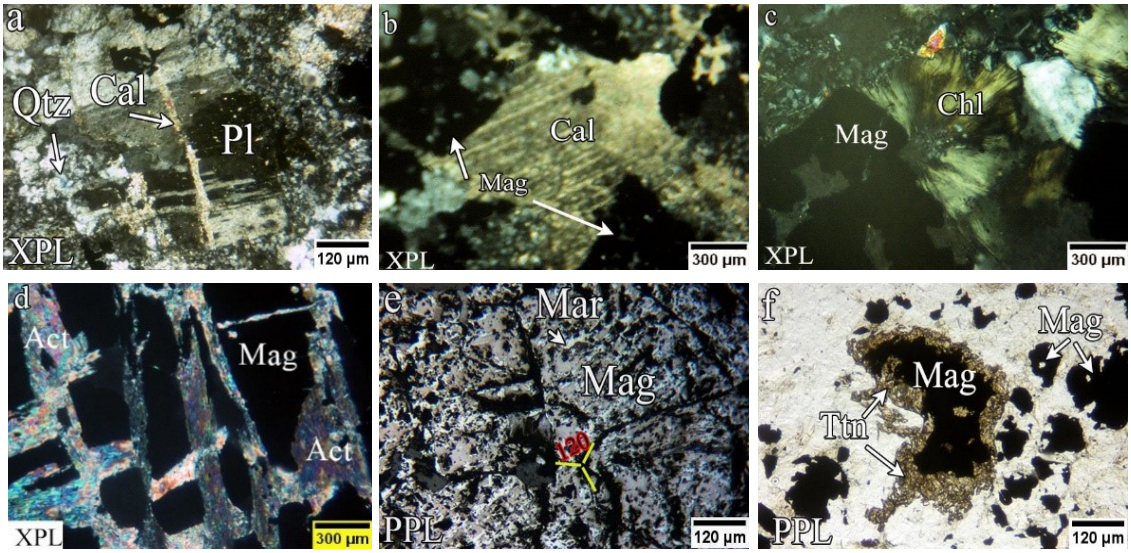


Fig 7. Photomicrographs (plane polarized light (PPL) and XPL) of: a. Spaces (fractures) between magnetite are filled by calcite b- c. Precipitated calcite and spherulitic chlorite as a post-impact hydrothermal activity. d. Intergrowth of actinolite with magnetite e. Fine-grained magnetite with angle of 120° between them (foam-like) and the martitization of grains border. f. Titanite as a rim on magnetite in the Sechahun and Choghart deposits

Generally, magnetite is partially or totally martitized due to hydrothermal alteration. Progressive martitization produces the perfect pseudomorphous magnetite to hematite that leaves magnetite or platy hematite to help identify the initial ore. Magnetite replacement by martite was followed by goethite-martite creation and predominance of goethite over martite. Goethite formed as irregular patches and net-like filler in fissures and open spaces. The iron ore enrichment by martite, goethite, and hydrous Fe oxides shows that various hydrothermal activities were responsible for the widespread alteration in this area. The green rocks and dolomites with thin intercalations of hematite and jaspilite crop out in the eastern highlands of the Sechahun area. Jaspilite units are folded, kinked, and locally faulted (Fig 8).


Fig 8. Field photo of cherry red jaspilite in the northeast part of the Sechahun deposit

The structural inventory indicates brittle to brittle-ductile behavior of the rocks under the low temperature/shallow conditions (Rosière and Chemale 2008). Jaspilite in the Sechahun area have no economic importance as noted by Förster and Jafarzadeh (1994). Primary high-temperature hematite seems to be absent in the main ore bodies and due to petrographic evidence, the secondary hematite may have various origins. Initial hematite along with martite formed by magnetite oxidation at the lower temperature near the surface. Platy specular hematite formed during the second stage, and at the final stage, modified fluids probably derived from the meteoric water; goethite is also widely distributed in the area. Apatite is not common in volcanic host rocks of the Sechahun deposit, but apatite and magnetite are the most abundant minerals in mineralized zone. Apatite has a coeval occurrence with the iron ore in the Bafq mining district. There are several generations for apatite in the Bafq district (Jami 2005; Torab 2008). Initial apatite enriched in REE, Na, and Si, but apatite II is recrystallized and has no REE, Na, and Si. Based on Torab (2008) after Ziemann et al. (2005), fluids chemistry and REE budget of the host fluorapatite are the main parameters for controlling monazite forming during hydrothermal overprint on fluorapatite. Pyrite is the most common sulphide mineral in the study area, although rare chalcopyrite is also found with pyrite. Subhedral to euhedral pyrite crystals are abundant, especially in the matrix of the ore breccia. Interaction between Fe-rich host rocks and S-bearing fluids would result in the pyrite formation. Chalcopyrite formed as small inclusions or disseminations in pyrite.

## 4. Material and Methods

To achieve the research goals, during several field trips a series of geological data were collected by systematic observation and sampling from the Sechahun ore bodies, host rocks, and some nearby iron-apatite deposits, such as Choghart and Gazestan (Sheytour) using outcrops and drill cores. The major and trace elements of volcanic and subvolcanic rocks (dykes and sills) were determined by X-ray fluorescence (XRF) and spectrometry methods. Whole rock lithogeochemical measurements were performed on typical drill core samples to characterize the host rocks of ore deposit. The results are presented in the tables 2 and 3. The REE-bearing minerals were obtained by magnetic separation and hand picking. All selected samples from the Sechahun and nearby deposits were analyzed for Rare Earth Elements using high resolution inductively coupled plasma-optical emission spectrometry (ICP–MS). The microthermometry of fluid inclusions was carried out mainly on the calcite veins from drill core samples within magnetite ore bodies. The measurements were focused on primary inclusions using a gas flow heating-freezing stage. Thermobarometry accomplished by heating and cooling stage of MDS600 with degree of diversity from -190 to 600+ $^{\circ}$C. Potassium dichromate was used for calibration of the device for the heating experiments and the standard fluorine for the cooling experiments.

## 5. Geochemistry

Classification of rock types has been carried out using the $Na_2O+K_2O$-$SiO_2$ diagram (Fig 9 and Table 2 and 3). The sample's range is 5 to 15 wt.% in combined alkalis and 47 to 75 wt.% in silica. The most acidic volcanic rocks plot within the rhyolite field. Tuffs have rhyolitic and dacitic compositions, while dykes plot within the basalt field. The high field strength elements, such as Zr, Ti, Nb, and Y, are relatively immobile during alteration and often used as indicators of the rock formation environment (Lacerda Filho, et al. 2016). Therefore, the samples are plotted in the rock classification diagram Nb/Y vs. Zr/Ti (modified by Pearce 1996; Fig 10) that indicates the rhyolite-dacite and trachyte composition of the volcanic rocks.

The average concentration of REEs in the apatite minerals of Sechahun, Choghart, and Gazestan (Table 4) in the Bafq mining district are compared with the rare earth abundance of Kiruna-type ore (Fig 11). The high amount of LREE/HREE ratio in these deposits indicates progressive magmatic differentiation (Eslamizadeh and Samanirad 2014). Observation of the similar patterns indicates their common origin. Comparing all samples show the LREE enrichment and a negative europium anomaly. The negative Eu anomaly was probably caused by discrimination of $Eu^{+2}$ and plagioclase fractionation during differentiation. Under the low-oxygen fugacities $Eu^{+2}$ substitutes by $Ca^{+2}$ in plagioclase or magnetite structures and this high degree of Eu fractionation separates it from other REE elements (Imchen et al. 2015). During albitization, a quantity of Eu was selectively fixed in the plagioclase structure, substituted for Ca that had already been leached, while other rare earth elements mobilized out of the rocks toward the hydrothermal system and subsequently situated at apatite structure of the magnetite-apatite ore. The origin of these deposits can be supposed either magmatic or hydrothermal. Consequently, both processes have probably been active. Study of rare earth elements of apatite and magnetite in Kiruna-type iron ores by Frietsch, and Perdahl (1995) indicates setting at an extensional rift environment for the iron ores that might originate from partial melting of deep-seated rocks on those apatite-iron ores formed by a late-magmatic differentiation.

The same source can be considered for the IOA deposits of Bafq due to similar geochemistry and REE pattern of apatite. The elements' concentration in bright and dark domains of apatite crystals in the Bafq district (Torab, 2008) and Sechahun (Bonyadi et al. 2011) is interpreted as resulting from a later hydrothermal overprint. Torab and Lehmann (2007) believed that the original REE pattern of these apatites has been obscured by a subsequent hydrothermal overprint. According to Knipping et al. (2015) trace elements in magnetite from massive iron oxide-apatite deposits indicate a combined formation by igneous and magmatic-hydrothermal processes, in which igneous magnetite is separated as fluid-magnetite aggregates from the silicate magma and become a rising suspension, based on its lower density relative to the surrounding magma. Such a phenomenon could have occurred in the magmatic evolution of Sechahun. However, it is necessary to study of the BSE images and EDS maps of the magnetite grains.

The similar REE pattern of the ore and the host rocks is likely because of the host rocks affected by the fluids caused this overprinting. The strong similarity is obvious in REE distribution in magnetite crystals of the Sechahun and Choghart deposits (Fig 12 and table 5).

The REE enrichment in Sechahun magnetite is probably due to a situation of some microscopic REE-bearing minerals in its lattice introduced by the late magmatic fluids.

## 6. Fluid inclusion investigation

Fluid inclusions in apatite investigated by Jami (2003) have indicated a significant role for fluids in the evolution of the Esfordi deposit, but do not preclude a role for immiscible Fe-oxide–P-rich melts in the initial stages of the mineralizing process. Also petrogenesis from geochemical, fluid inclusion, and sulfur isotope data of Chadormalu has done by Heidarian et al. (2017), dissecting the petrogeochemical systems, but for a magmatic fluid to saline meteoric fluid mixing system, rather than an immiscible Fe-P fractionated mafic magmatic system to saline meteoric hydrothermal system.

Table 2. X-Ray Fluorescence analyses of rocks from the Sechahun deposit.

| Sample(Wt%) | $SiO_2$ | $Al_2O_3$ | $Fe_2O_3$ | CaO | $Na_2O$ | $K_2O$ | MgO | $TiO_2$ | MnO | $P_2O_5$ |
|---|---|---|---|---|---|---|---|---|---|---|
| **1** | 66.4 | 12.3 | 2.42 | 1.4 | 9.95 | 3.9 | 1.1 | 0.17 | 0.05 | 0.05 |
| **2** | 59.9 | 8.8 | 11.2 | 2.1 | 4.7 | 3.8 | 6.3 | 0.19 | 0.07 | 0.05 |
| **3** | 67.3 | 14.2 | 1.61 | 1.5 | 7.85 | 3.4 | 2.5 | 0.15 | 0.04 | 0.03 |
| **4** | 65.9 | 18.4 | 1.34 | 1.5 | 9.05 | 3.8 | 0.6 | 0.17 | 0.05 | 0.01 |
| **5** | 70.3 | 13.8 | 3.22 | 1.8 | 4.91 | 4.1 | 1.9 | 0.17 | 0.05 | 0.08 |
| **6** | 71.8 | 14.2 | 2.93 | 1.8 | 4.02 | 2 | 1.5 | 0.21 | 0.07 | 0.09 |
| **7** | 71.3 | 11.9 | 2.27 | 3 | 3.43 | 5 | 2 | 0.23 | 0.06 | 0.08 |
| **8** | 56.8 | 9.43 | 13.34 | 3.2 | 4.44 | 3.8 | 6.2 | 0.18 | 0.11 | 0.06 |
| **9** | 58.4 | 9.78 | 11.21 | 4.3 | 5.21 | 3.1 | 5.5 | 0.17 | 0.09 | 0.06 |
| **10** | 67.1 | 13.5 | 1.66 | 1.4 | 8.12 | 2.5 | 1.6 | 0.18 | 0.06 | 0.07 |
| **11** | 47.4 | 13.3 | 13.17 | 8.5 | 2.45 | 1.8 | 7.9 | 3.27 | 0.32 | 0.48 |
| **12** | 67.7 | 18.2 | 0.05 | 1.8 | 2.82 | 2.2 | 3.1 | 0.02 | 5.14 | 0.02 |
| **13** | 73.3 | 12.2 | 0.04 | 1.6 | 0.88 | 6.9 | 1 | 0.01 | 0.3 | 0.01 |
| **14** | 75.9 | 13.4 | 0.05 | 1.3 | 1.76 | 7 | 1 | 0.03 | 0.25 | 0.01 |
| **15** | 72.7 | 13.6 | 0.02 | 2.5 | 1.02 | 3.3 | 1.5 | 0.09 | 3.82 | 0.01 |
| **16** | 74.8 | 12 | 0.64 | 2.5 | 0.67 | 7.6 | 0.9 | 0.18 | 0.02 | 0.03 |
| **17 S** | 65.86 | 18.37 | 1.34 | 1.46 | 9.05 | 3.78 | 0.62 | 0.01 | 0.01 | 0.01 |

Table 3. Trace element's distribution in selected host rocks of the Sechahun deposit (with a XRF detection of ppm).

| Sample (ppm) | AS01 | AS02 | AS03 | AS04 | AS05 | AS06 | AS07 | AS08 | AS09 | AS10 |
|---|---|---|---|---|---|---|---|---|---|---|
| **S** | 27.1 | 59 | 1.02 | 52 | 32 | 14 | 13 | 23 | 1 | 42 |
| **Cl** | 76 | 28 | 27 | 67 | 36 | 45 | 57 | 74 | 37 | 87 |
| **Ba** | 822 | 425 | 757 | 380 | 213 | 281 | 566 | 612 | 636 | 491 |
| **Sr** | 728 | 655 | 829 | 412 | 741 | 522 | 421 | 531 | 500 | 633 |
| **Cu** | 13.0 | 52.3 | 45.3 | 44.1 | 12.2 | 13.5 | 17.7 | 13.4 | 15.2 | 14.3 |
| **Zn** | 70.3 | 194 | 171 | 110 | 101 | 90.7 | 61.2 | 90.3 | 155 | 54.4 |
| **Pb** | 9.7 | 13.5 | 16.3 | 14.2 | 6.5 | 5.0 | 5.7 | 6.3 | 28.2 | 9.3 |
| **Ni** | 14.9 | 13.8 | 33.8 | 31.5 | 17.4 | 30.6 | 41.9 | 15.2 | 12.2 | 17.7 |
| **Cr** | 55.9 | 44.1 | 80.3 | 23.9 | 46.9 | 43.7 | 67.3 | 34.7 | 12 | 61.8 |
| **V** | 153 | 227 | 236 | 206 | 65 | 52.2 | 82 | 37.6 | 27.3 | 148 |
| **Ce** | 68.3 | 179 | 181 | 20.8 | 64.3 | 55.7 | 67.4 | 48.7 | 54.3 | 170 |
| **La** | 444 | 323 | 154 | 98.5 | 236 | 249 | 211 | 398 | 126 | 73.6 |
| **W** | 7.9 | 3.7 | 1.7 | 4.1 | 7.5 | 4.3 | 4.6 | 3.8 | 1.5 | 8.3 |
| **Zr** | 176 | 332 | 355 | 90 | 191 | 156 | 136 | 145 | 90.6 | 115 |
| **Y** | 57.4 | 45.8 | 15.7 | 45.3 | 24.6 | 17.6 | 37.9 | 65.6 | 16.3 | 19 |
| **Rb** | 94.8 | 87.9 | 86.9 | 35.8 | 49.3 | 76.4 | 97.7 | 85.9 | 85 | 67.9 |
| **Co** | 15 | 34.6 | 76.4 | 67.9 | 5.8 | 33 | 8.3 | 3.5 | 35.8 | 43 |
| **As** | 4.6 | 5.7 | 6.2 | 0.13 | 3.7 | 5.9 | 4.3 | 4.3 | 12.7 | 4.3 |
| **U** | 7.3 | 14.3 | 18 | 9.4 | 8.7 | 4.3 | 17.3 | 20.8 | 20.5 | 16.9 |
| **Th** | 14.7 | 15.0 | 17.7 | 15.6 | 31.1 | 8.9 | 15.2 | 13.8 | 7.2 | 50 |
| **Mo** | 6.9 | 2.2 | 5.3 | 7.8 | 8.4 | 7.0 | 4.0 | 8.4 | 5.2 | 9.7 |
| **Ga** | 6.9 | 18.3 | 10.6 | 13.2 | 10.5 | 6.7 | 13.4 | 15.2 | 11.2 | 2.1 |
| **Nb** | 23.2 | 12.9 | 25.2 | 11.3 | 7.0 | 8.9 | 16.4 | 17.3 | 16.5 | 15.2 |

The fluid inclusion determination on vein calcite-magnetite samples from drill core of Sechahun was done to study the general aspects of hydrothermal alteration processes. The thin–polished sections were studied under a Nikon microscope with 10x-50x-100x objective lenses in Geological Survey & Mineral Explorations of Iran (GSI). Thermo-barometry accomplished by cooling and heating stage of MDS600 with degree of diversity from $^{-}$190 to $^{+}$600°C. The primary fluid inclusions formed during growth of the surrounding host crystal when fluid is trapped on the active growing surface of a crystal. (Roedder 1984; Goldstein 2003). The study of the primary fluid inclusions of the Sechahun deposits, indicates four types of inclusions (table 5 and Fig 13). The solid-rich fluid inclusions (L+V+S) have a high salinity. The liquid-dominated fluid inclusions with minor vapor (70-90%L+10-30% V) and a salinity between 1-21 wt.% NaCl equivalent, are the most abundant inclusions, which locally containing hematite crystals. $CO_2$-rich vapor inclusions are usually rare. The single vapor inclusions resulted from boiling conditions and entrapment.

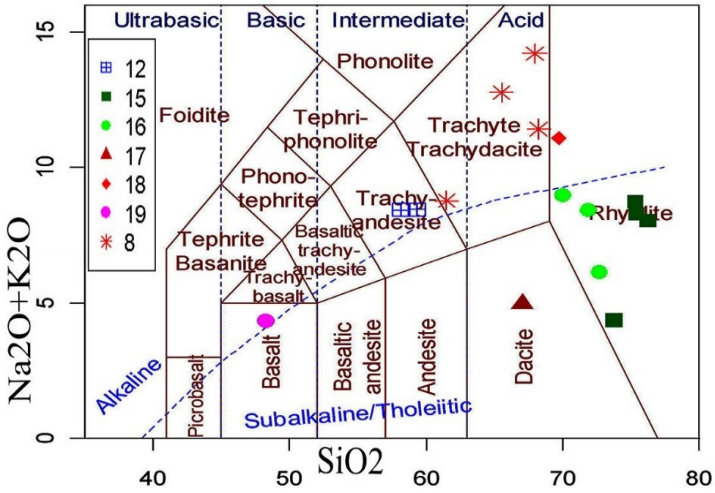


Fig 9. Samples plot in the total alkali vs. silica diagram (Le Bas et al. 1986). The rocks have a composition of: Trachyandesite (12), Rhyolitic tuff (15), Rhyolite (16), Dacitic tuff (17), Trachy-dacite (18), Trachyte (8), and diabasic dyke (19).

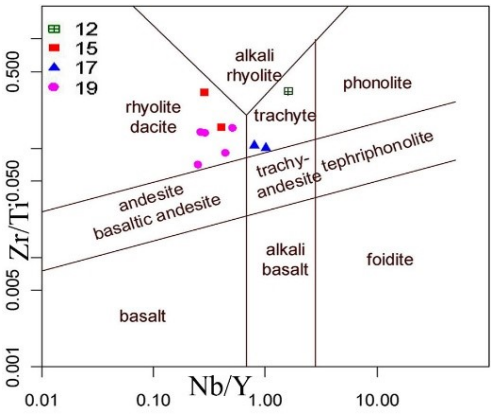


Fig 10. Plot of Nb/Y versus Zr/Ti (modified by Pearce 1996) indicates the rhyolite-dacite (15, 19) and trachyte (12, 17) composition of the volcanic rocks.

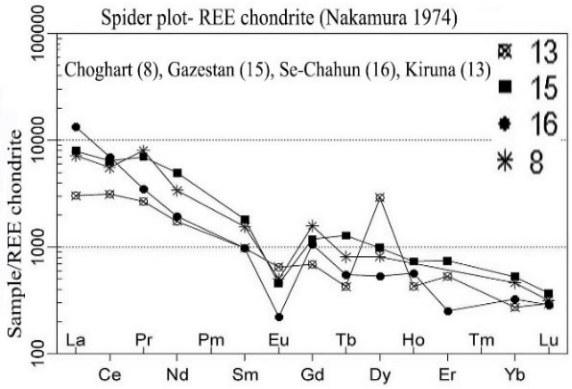


Fig 11. Chondrite-normalized REE distribution in apatite from Sechahun, Choghart, Gazestan deposits, with data chondrite after Nakamura (1974); these are compared with Kiruna-type ore (data from Frietsch and Perdahl 1995).

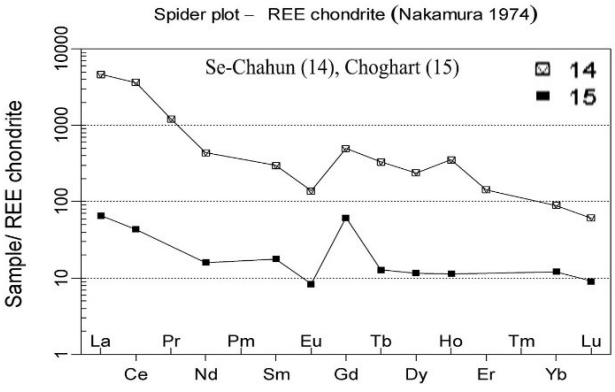


Fig 12. Rare earth abundance in magnetite of Sechahun and Choghart indicate the same pattern with higher REE content of the Sechahun deposit.

The results of primary fluid inclusions analysis are summarized in table 5. There are different scopes of salinity from 1.32 to more than 54 wt% of NaCl and the liquid density varies from 0.4 to 1.2 g/cm$^3$. It is interpreted as an influence of different types of the ore-bearing fluids from high to moderate salinity. The homogenization temperature of three phase inclusions, change from 395 to 485° C, indicating presence of other salts besides of NaCl in the mineralizing fluids from the Sechahun deposit. In the homogenization temperature histogram (Fig 14), the temperature varies from 146 to 486°C and the most frequency of the homogeneous temperature is related to two-phase inclusions (V+L), from 200 to 350°C. The diagram of homogenization temperatures vs. salinity and density of fluid inclusions (Fig 15) is used for determining the density variation and the evolution of ore-bearing fluids in the Sechahun deposit. As presented in this diagram, the density changes from 0.5 to 0.9 g/cm$^3$, and the reduction of homogenization temperature cause an increase in density. Based on Wilkinson (2001), the reduction of temperature and mixture of fluids precipitates the ores. The low density of two phases predominated inclusions of Sechahun is evidence of two fluids mixing and the impact of hydrothermal activity to precipitating the ore deposit. The homogenization temperatures of two-phase inclusions in the Sechahun deposit, based on their salinities, change from 200° to 450°C (Fig 16), but most of them are plotted between 200° to 350°C.

Table 4. Average REE abundance (ppm) in apatite and magnetite of Sechahun, Choghart, and Gazestan ore deposits (ICP-MS analyses).

| Sample | Sechahun | Choghart | Gazestan | Choghart | Sechahun |
|---|---|---|---|---|---|
| ppm | Apatite | Apatite | Apatite | Magnetite | Magnetite |
| La | 4416.7 | 2366.7 | 2620 | 439 | 3767.5 |
| Ce | 5590 | 4800 | 5532 | 796 | 5980 |
| Pr | 390.5 | 895.0 | 785.0 | | 181.8 |
| Nd | 1224.7 | 2133.3 | 3120.0 | 318.0 | 511.9 |
| Sm | 197.3 | 314.7 | 368.0 | 44.9 | 118.4 |
| Eu | 17.1 | 38.9 | 35.2 | 4.0 | 16.0 |
| Gd | 291.2 | 436.0 | 327.6 | | 188.5 |
| Tb | 25.9 | 38.0 | 60.3 | | 19.2 |
| Dy | 181.9 | 278.3 | 337.0 | 26.3 | 117.0 |
| Ho | 40.1 | 0 | 51.4 | | 24.45 |
| Er | 56.6 | 0 | 167.0 | | 43.5 |
| Yb | 72.0 | 101.8 | 116.0 | 9.3 | 37.0 |
| Lu | 9.7 | 10.8 | 12.5 | 1.27 | 4.39 |
| ΣREE% | 1.29 | 1.14 | 1.35 | 0.16 | 1.10 |

Table 5. Summarized results of primary fluid inclusions analysis in the Sechahun deposit

| Code | Type | Class | Fill | Tm-ice | Ts_hal | Th-aq | Tm-Clathrate | Phase | EqWt% Salinity | Density |
|---|---|---|---|---|---|---|---|---|---|---|
| GH1 | V+L | primary | 0.83 | -7.4 | | 397 | | Liquid | 10.98 | 0.68 |
| GH2 | V+L | primary | 0.75 | -0.8 | | 378 | | Liquid | **1.32** | 0.54 |
| GH3 | V+L | primary | 0.59 | -3.7 | | 468 | | Liquid | 5.93 | **0.41** |
| GH10 | V+L+S | primary | 0.79 | | **458** | 386 | | Liquid | **54.26** | **1.19** |
| GH11 | V+L | primary | 0.69 | -10.2 | | 439 | | Liquid | 14.26 | 0.66 |
| GH14 | V+L+S | primary | 0.65 | | **395** | 336 | 10.5 | Liquid | 43.25 | **1.11** |
| GH33 | V+L | primary | 0.81 | -2.5 | | 275 | | Liquid | 4.07 | 0.79 |
| GH34 | V+L | primary | 0.87 | -9.6 | | 227 | | Liquid | 13.52 | 0.94 |
| GH35 | V+L | primary | 0.93 | -3.9 | | 301 | | Liquid | 6.23 | 0.78 |

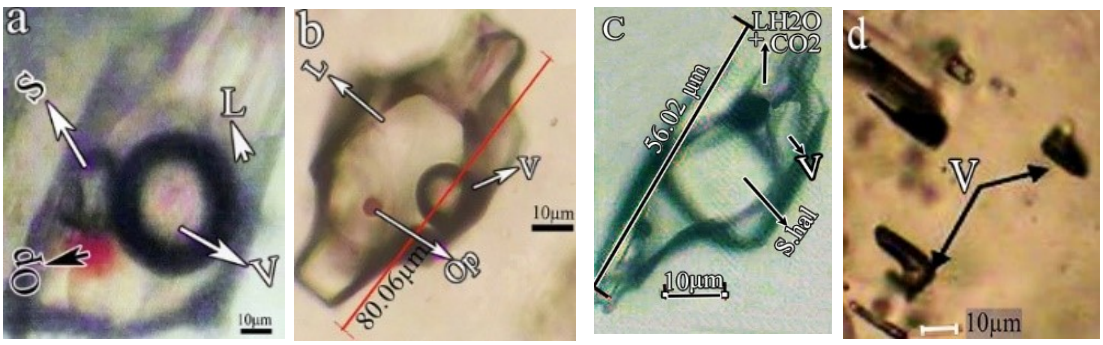


Fig 13. Photomicrographs of four types of the primary inclusions: a. Three-phase inclusions (L+V+S), b. The liquid-dominated inclusions (L+V) with minor vapor contain crystals of hematite (Op), c. $CO_2$-rich vapor inclusions (CO2+V+S). d. The single vapor inclusions (V).

As noted by Pirajno (2009), hydrothermal mineral deposit forms by the circulation of warm to hot fluids (about 50 to > 500°C) that leach, transport, and subsequently precipitate their mineral load in response to changing physico-chemical conditions.

The possible deep trapping of inclusions is estimated by using the pressure-temperature chart (Roedder 1984) in Fig 17. The dashed line shows the minimal pressure of 30 bars in depth of 200 meters to a pressure of 450 bars and depth of 4500 meters for trapping of fluid inclusions of the Sechahun deposit, based on their homogenization temperatures. The origin of fluids is defined by using the salinity- homogenization temperature diagram designed by Roedder (1984) and Wilkinson (2001). Based on this diagram (Fig 18), the majority of fluid inclusion's plot in the seawater field showing the most important role of hydrothermal solution. Only a few of them plot in the magmatic field indicating the role of both magmatic and hydrothermal fluids.

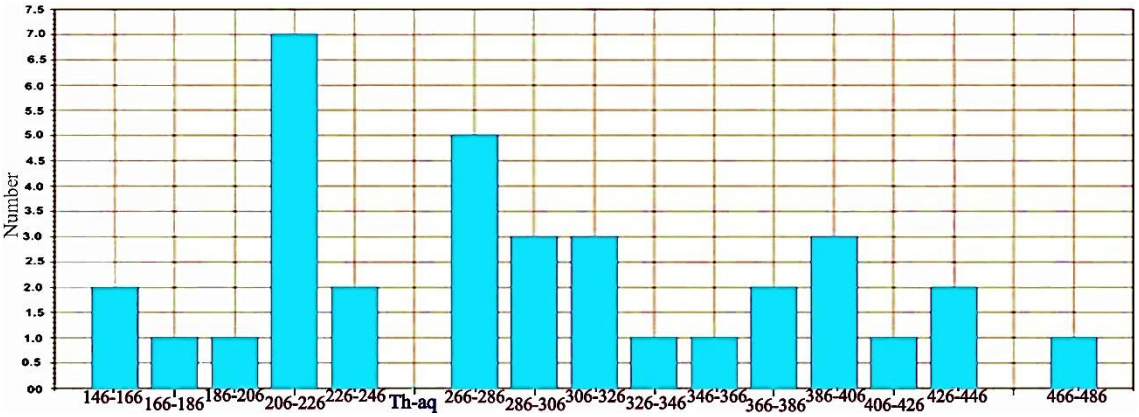


Fig 14. Fluid inclusion homogenization temperature histogram (°C)

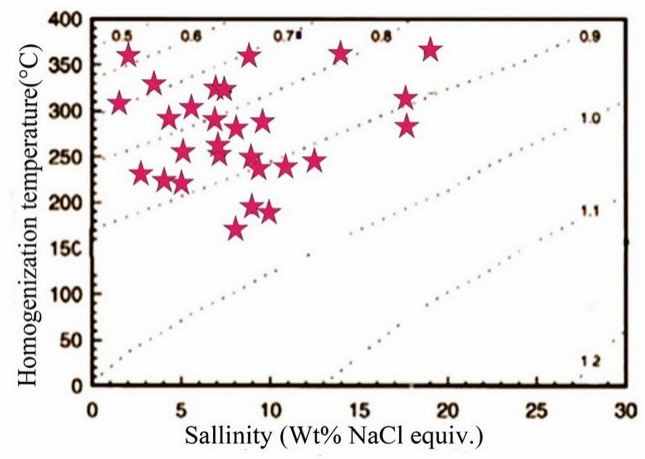


Fig 15. Density variation versus temperature and salinity of fluid inclusions from the Sechahun deposit, based on Wilkinson (2001) shows the density changes from 0.5 to 0.9 g/cm$^3$.

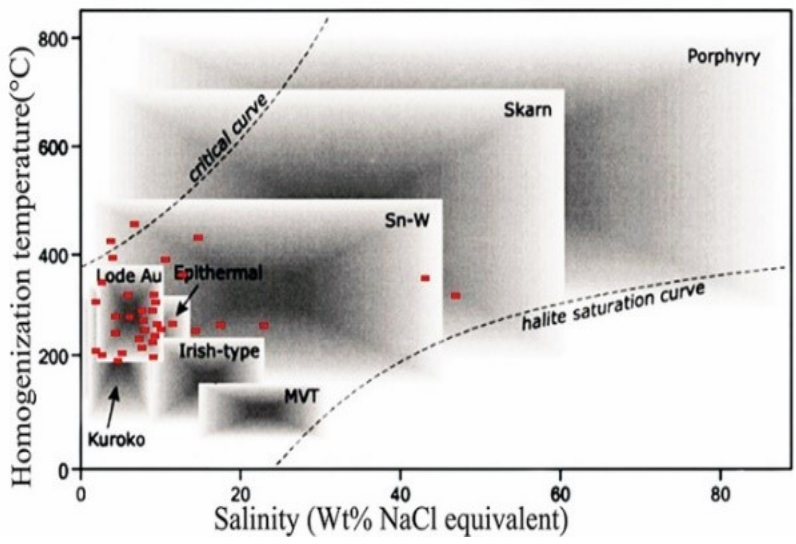


Fig 16. Most samples plot in the field of 200 to 350 °C indicating a mesothermal fluid (modified after Wilkinson, 2001).

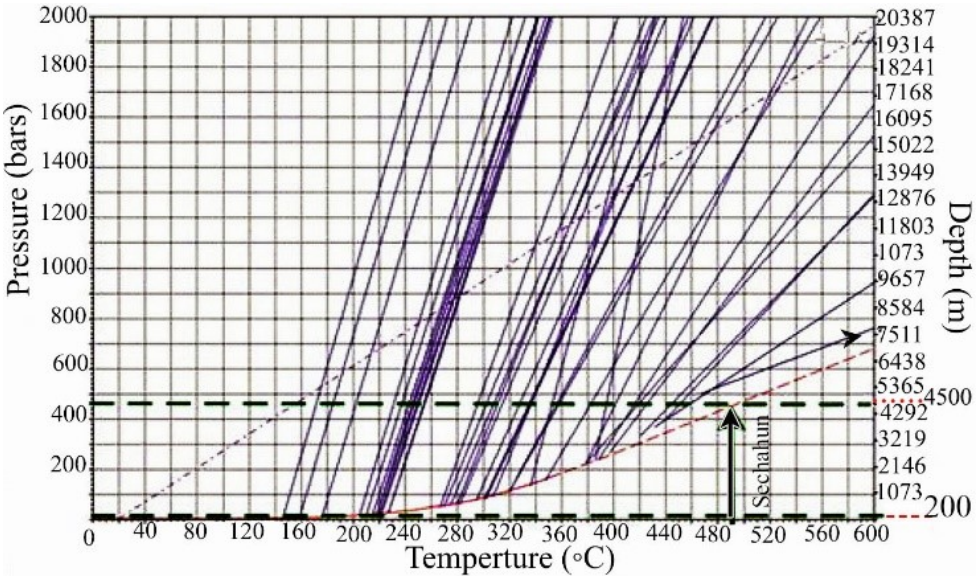


Fig 17. P-T diagram with dashed line shows the minimal pressure for trapping of fluid inclusions from the Sechahun deposit, based on their homogenization temperatures (modified after Roedder 1984).

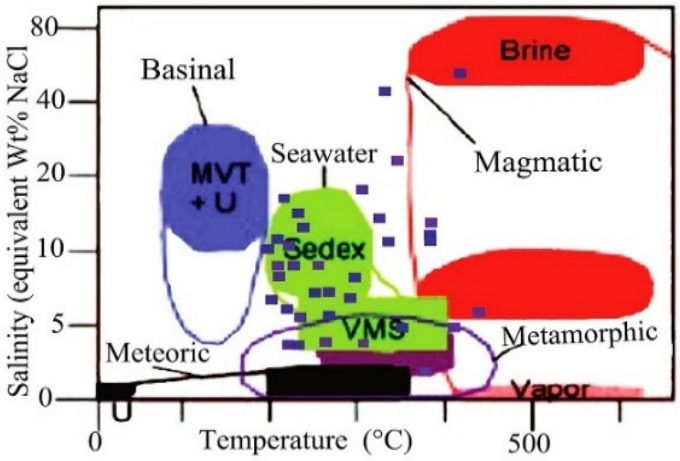


Fig 18. Homogenization temperature versus salinity of fluid inclusions (modified after Roeder 1984 and Wilkinson 2001), shows the majority of fluid inclusion's plot in the sea water field.

However, hydrothermal fluids were more important and active. It is concluded that hydrothermal process has a significant role (rather than metasomatic factors) in creation of the widespread intrusion-related vein-type ore bodies due to magmatic activity during the back-arc rifting. These ore bodies are assumed to be related to mesothermal systems, which may be related to circulation of hydrothermal fluids driven by heat energy associated with the emplacement of mafic dykes of the large magmatic province (Pirajno 2004).

## 7. Discussion

Relation between the ores and their host rocks of iron-oxide apatite deposits (IOA Kiruna-type) of Bafq, including Sechahun, has been subject of discussion for many years. The main argument is over the fact that there is no evidence the iron was extracted from the volcanic host rocks, since they are free of iron-bearing minerals. There are mafic and ultramafic rocks, such as pyroxenite in Choghart deposit (Eslamizadeh and Samanirad 2013) and gabbro intrusions in Esfordi and Chagas (Rajabi et al. 2015), as host the mineralization.

Daliran (1990) proposed a volcanic–exhalative ore-forming process for Mishdovan and added the crystal growth of the paragenetically associated apatite, and its REE pattern correlated with a magmatic origin. The Bafq mining district was investigated by Förster and Jafarzadeh (1994), as a highly mineralized Infracambrian volcanic field in that magmatic material produced from magma differentiation and liquid immiscibility of a melanephelinitic melt. By considering this statement, doubt about the rhyolitic parental magma still remains. Therefore, a plausible source could be a magmatic differentiation model originating from the upper mantle in which the IOA deposits were emplaced at various crustal depths. The hydrothermal activities caused the alteration and brecciation of the host volcanic rocks. At the mesothermal to epithermal conditions in the subaqueous near-surface environment the hematite-jaspilite bearing rocks formed. The host volcanic rocks have formed at the root zone of a caldera at shallower environment. Bimodal volcanism (Daliran and Stosch 2007) associated with the continental back-arc rifting during the Late Neoproterozoic-Early Cambrian (Rajabi et al. 2015), and emplacement of highly fractionated melts along the regional fracture and fault lines are controllers for Fe-P mineralization in the Bafq district. During rifting, as mentioned by Frietsch (1984) and Nystrom and Henriques (1994), the intrusion occurs as high-temperature process and the original magma segregates through a fractionation of early formed magnetite crystals. Due to evidence of petrology and geochemistry, two processes can be considered for the magmatic evolution in the Sechahun area. At the first stage, circulation of deuteric solutions within the surrounded rocks released a large amount of $CO_2$, F, P, Fe, Mg, Ca, Na, and other metal ions. As a result, quartz and feldspar-bearing rocks remained. Migration of heated mineralization fluids at the later stages, precipitated soluble Fe as magnetite ore deposits. A large amount of tremolite-actinolite formed by Mg, and Ca content of fluids created intergrown dendritic crystals with magnetite. The general characteristics of the Sechahun iron-oxide apatite deposit can be summarized as Table 6. Finally, the mineralogical, textural, and compositional diversity in all rock types of the study area caused by circulating hydrothermal fluids through replacement and extensive hydrothermal alteration.

Table 6. General characteristics of the IOA deposits in the Bafq mining district

| Characteristics | Iron-oxide apatite (*IOA Kiruna type*) |
|---|---|
| **Age** | Early Cambrian (539 to 527 Ma) |
| **Tectonic setting** | Continental margin back-arc rifting, parallel to convergence (Proto-Tethyan) along the continental margin. |
| **Host rock** | Calc–alkaline to alkaline volcanic rocks |
| **Morphology** | Massive, brecciated and impregnated ore with lava flow, sill, dyke and pyroclastic material |
| **Mineralogy** | Magnetite –Apatite –martite and quartz, Albite, actinolite, calcite |
| **Alteration** | Albitization, sericitization, silicification, chloritization and actinolitization |
| **Ore genesis** | Magmatic intrusive/extrusive and hydrothermal replacement. |

## 8. Conclusions

The iron oxide- apatite deposits overlay the felsic volcanic rocks and altered vitric tuffs in Sechahun. Carbonates, green rocks, and shale are predominant units in this area. Distribution pattern of REE in apatite minerals is similar to the Kiruna-type ores. The iron ore occurrence is limited to the Early Cambrian Rizu Formation. Hydrothermal alteration is widespread in the study area. The sodic, potassic, and calcic overprint caused mineralogical and textural changes in all rock types. The chessboard albite that is the main feldspar in syenitic sills shows metasomatic factors. Diabasic dykes are numerous and widespread. The most iron ore bodies contain apatite. Ilmenite exsolution with magnetite and dendritic intergrowth of magnetite and actinolite indicates a magmatic source for these minerals. Fluid inclusion study indicates an important role of hydrothermal activity in evolution of the Sechahun IOA deposit. The magmatic-hydrothermal IOA deposits were emplaced at different depths. A combined magmatic hydrothermal to convective hydrothermal model defined for generation the plausible source of iron in this area. Magmatic events occurred as the high-temperature process during rifting and highly fractionated melt along the regional fracture-fault lines.

## Acknowledgments

The manuscript was greatly improved from earlier comments and technical editing of professor David Lentz (University of New Brunswick). I would also like to express my gratitude to the anonymous reviewers and thanks for helpful comments, valuable suggestions, and critical reading of an early version of the manuscript that helped to improve the paper significantly. They do not bear any responsibility for the errors of fact or interpretation that may still remain in this paper.

## References

Berberian M, King GC (1981) Towards a paleogeography and tectonic evolution of Iran. *Canadian Journal of Earth Sciences* 18: 210-265.

Barton MD, Johnson DA (1996) Evaporitic-source model for igneous-related Fe oxide -REE-Cu-Au-U) mineralization. *Geology* 24: 259-262.

Bonyadi Z, Davidson GJ, Mehrabi B, Meffre S, Ghazban F (2011) Significance of apatite REE depletion and monazite inclusions in the brecciated Se–Chahun iron oxide–apatite deposit, Bafq district, Iran: insights from paragenesis and geochemistry. *Chemical Geology* 281: 253-269.

Daliran F (1990) The magnetite –apatite deposit of Mishdovan, East Central Iran*, Ph.D. Thesis*, Univ. of Heidelberg. Geowiss. Abhandl, 248p.

Daliran F (2002) Kiruna-type iron oxide-apatite ores and apatitites of the Bafq district, Iran, with an emphasis on the REE geochemistry of their apatites. In: Porter, T.M. (Ed.), Hydrothermal Iron Oxide Copper-Gold and Related Deposits: A Global Perspective, vol. 2. *PGC Publishing*, Adelaide, pp. 303–320.

Daliran F, Stosch HG, Williams P, Jamali H, Dorri MB (2010) Early Cambrian iron oxide-apatite-REE (U) deposits of the Bafq District, east-central Iran. Exploring for Iron oxide copper–gold deposits: Canada and Global analogues. *Geol Assoc Canada*, Short Course Notes 20: 143- 155.

Daliran F, Stosch HG, Williams P (2007) Multistage metasomatism and mineralization at hydrothermal Fe oxide-REE-apatite deposits and "apatitites" of the Bafq District, Central-East Iran. *The 9th Biennial Meeting of the Society for Geology Applied to Mineral Deposits*, Dublin, 1501-1504.

Daliran F, Stosch HG, Williams PJ (2009) A review of the Early Cambrian magmatic and metasomatic events and their bearing on the genesis of the Fe oxide-REE-apatite deposits (IOA) of the Bafq district, Iran. In: Williams P (Ed.): Smart Science for Exploration and Mining. *10th SGA Biennial, Townsville*, 623–625

Eslamizadeh A (2017) Petrology and Geochemistry of Early Cambrian Volcanic Rocks Hosting the Kiruna-type Iron Ore in Anomaly 10 of Sechahun, Central Iran. *Journal of Sciences*, 28(1): 21 - 35

Eslamizadeh A, Akbarian N (2015) Mineralogy and Classification of Altered Host Rocks in the Zaghia Iron Oxide Deposit, East of Bafq, Central Iran. World Academy of Science, Engineering and Technology, International Science Index, *Geological and Environmental Engineering* 17: 2673-2677.

Eslamizadeh A, Samanirad Sh (2013) Atlas of rocks and minerals from iron ore mines in central Iran. Iran Central Iron Ore Co. Bafgh, *research project*, 294 p. (in Persian).

Eslamizadeh A, Samanirad Sh (2014) Distribution of rare earth elements in the iron oxide- apatite (IOA) deposits of the Bafgh mining district, *Central Iran, the 32nd National & the 1st International Geosciences Congress*.

Eslamizadeh A, Samanirad Sh (2016) Petrography and Geochemistry of the REE-bearing Fe-Oxide-Apatite Assemblages from the Sheytour Deposit East Central Iran, *3rd International conference on research in engineering*, science and technology, Batumi, Georgia.

Förster H, Jafarzadeh A (1994) The Bafq mining district in Central Iran: a highly mineralized Infracambrian volcanic field. *Economic Geology* 89: 1697–1721.

Frietsch R (1984) on the magmatic origin of iron ore of the Kiruna Type- A reply. *Economic Geology* 79: 1949-1951.

Frietsch R, Perdahl JA (1995) Rare earth elements in apatite and magnetite in Kiruna-type iron ores and some other iron ore types. *Ore Geology Reviews* 9:489-510.

Gandhi SS (2003) An overview of the Fe oxide–Cu–Au deposits and related deposit types. CIM Montréal 2003 Mining Industry Conference and Exhibition, Canadian Institute of Mining, *Technical Paper*, CD-ROM.

Goldstein RH (2003) Petrographic analysis of fluid inclusions. Mineral. Assoc. Can., *Short Course Ser*. 32: 9-53.

Groves DI, Bierlein FP, Meinert LD, Hitzman MW (2010) Iron oxide copper-gold (IOCG) deposits through earth history: implications for origin, lithospheric setting, and distinction from other epigenetic iron oxide deposits. *Economic Geology* 105: 641-654.

Heidarian H, Alirezaei S, Lentz, DR (2017) Chadormalu Kiruna-type magnetite-apatite deposit, Bafq district, Iran: Insights into hydrothermal alteration and petrogenesis from geochemical, fluid inclusion, and sulfur isotope data. *Ore Geology Review* 83: 43–62

Hitzman MW (2000) Iron Oxide-Cu-Au deposits: what, where, when, and why, in Porter, T M ed, Hydrothermal iron oxide copper-gold & related deposits: A global perspective: *PGC Publishing*, Adelaide 1: 9-25.

Hushmandzadeh A (1989) An introduction to the geology of the Biabanak-Bafgh region. *Proceeding of the seminar on reserves and mining potential of the Yazd department 1988*. Ministry of Mines and Metals 341-371 (in Farsi).

Imchen W, Patil SK, Rino V, Thong GT, Pongen T, Rao BV (2015) Geochemistry, petrography and rock magnetism of the basalts of Phek district, Nagaland. *Current Science* 108: 2240.

Jami M (2005) Geology, geochemistry and evolution of the Esfordi phosphate-iron deposit, Bafq area, Central Iran. *Unpublished PhD Thesis*, The University of New South Wales, Australia.

Jami M, Dunlop AC, Cohen DR (2009) Fluid Inclusion and Stable Isotope Study of the Esfordi Apatite-Magnetite Deposit, Central Iran-A reply. *Economic Geology* 104: 140-143.

Kinnaird JA (1985) Hydrothermal alteration and mineralization of the alkaline anorogenic ring complexes of Nigeria. *Journal of African Earth Sciences* 3: 229–252

Knipping JL, Bilenker LD, Simon AC, Reich M, Barra F, Deditius AP, Wälle M, Heinrich CA, Holtz F, Munizaga R (2015) Trace elements in magnetite from massive iron oxide-apatite deposits indicate a combined formation by igneous and magmatic-hydrothermal processes. *Geochimica et Cosmochimica Acta* 171: 15-38.

Lacerda Filho JV, Fuck RA, Ruiz AS, Dantas EL, Scandolara JE, Rodrigues JB, Nascimento NDC (2016) Paleoproterozoic tectonic evolution of the Alto Tererê Group, southernmost Amazonian Craton, based on field mapping, zircon dating and rock geochemistry. *Journal of South American Earth Sciences* 65: 122-141.

Liu PP, Zhou MF, Chen WT, Gao JF, Huang XW (2015) In-situ LA-ICP-MS trace elemental analyses of magnetite: Fe–Ti–(V) oxide-bearing mafic–ultramafic layered intrusions of the Emeishan Large Igneous Province, SW China. *Ore Geology Reviews* 65: 853-871.

Mohseni S, Aftabi A (2012) Comment on "Significance of apatite REE depletion and monazite inclusions in the brecciated Sechahun iron oxide–apatite deposit, Bafq district, Iran: Insights from paragenesis and geochemistry" by Bonyadi Z, Davidson GJ, Mehrabi B, Meffre S, Ghazban F, . *Chemical Geology* 334: 378-381.

Nabatian G, Rastad E, Neubauer F, Honarmand M, Ghaderi M (2015) Iron and Fe-Mn mineralization in Iran: implications for Tethyan metallogeny. *Australian Journal of Earth Sciences* 62: 211-241.

Nakamura N (1974) Determination of REE, Ba, Fe, Mg, Na and K in carbonaceous and ordinary chondrites. *Geochimica et Cosmochimica Acta* 38: 757-775.

Norberg N, Harlov D, Neusser G, Wirth, R, Rhede D (2014) Element mobilization during feldspar metasomatism: an experimental study. *European Journal of Mineralogy* 26(1): 71-82.

Nystrsm JO, Henriquez F (1994) Magmatic features of iron ores of the Kiruna type in Chile and Sweden. ore textures and magnetite geochemistry. *Economic Geology* 89: 820-839.

Pearce J (1996) Sources and settings of granitic rocks. *Episodes* 19: 120–125.

Pirajno F (2004) Oceanic plateau accretion onto the northwestern margin of the Yilgarn Craton, Western Australia: implications for a mantle plume event at ca. 2.0 Ga. *Journal of Geodynamics* 37:205–231.

Pirajno F (2009) Hydrothermal Processes and Mineral Systems, *Springer Netherlands*, 1097-1130.

Pollard PJ (1983) Magmatic and post magmatic processes in the formation of rocks associated with rare element deposits. *Trans Inst Min Metall* 92: B1–B9.

Rajabi A, Canet C, Rastad E, Alfonso P (2015) Basin evolution and stratigraphic correlation of sedimentary-exhalative Zn–Pb deposits of the early Cambrian Zarigan–Chahmir Basin, Central Iran. *Ore Geology Reviews* 64: 328-353.

Ramezani J, Tucker RD (2003) The Saghand region, Central Iran: U-Pb geochronology, petrogenesis and implications for Gondwana tectonics. *American Journal of Science* 303: 622-665.

Roedder E (1984) Fluid inclusions as tools in mineral exploration. *Economic Geology* 72: 503-525.

Rosière CA, Chemale Jr F (2008) Brazilian iron formations and their geological setting. *Brazilian Journal of Geology* 30: -278.

Sabet-Mobarhan-Talab A, Alinia F, Ghannadpour SS, Hezarkhani A (2015) Geology, geochemistry, and some genetic discussion of the Chador-Malu iron oxide-apatite deposit, Bafq District, Central Iran. *Arabian Journal of Geosciences* 8: 8399-8418.

Samani BA (1998a) Metallogeny of the Precambrian in Iran. *Precambrian Research* 39: 85-106

Samani BA (1998b) Recognition of uraniferous provinces from the Precambrian of Iran. *Krystalinikum* 19:147-65

Siivola J, Schmid R (2007) List of mineral abbreviations. Metamorphic Rocks: A Classification and Glossary of Terms. *Recommendations of the International Union of Geological Sciences Subcommission on the Systematics of Metamorphic Rocks* 93-110.

Stosch HG, Romer RL, Daliran F, Rhede D (2011) Uranium–lead ages of apatite from iron oxide ores of the Bafq District, East-Central Iran. *Miner Deposita* 46: 9–21.

Talbot CJ, Alavi M (1996) The past of a future syntaxis across the Zagros. Geological Society, London, *Special Publications* 100:89-109.

Torab FM (2008), Geochemistry and Metallogeny of Magnetite Apatite Deposits of the Bafq Mining District, Central Iran. (Doctoral dissertation, Papierflieger).

Torab FM, Lehmann B (2007) Magnetite-apatite deposits of the Bafq district, Central Iran: apatite geochemistry and monazite geochronology. *Mineralogical Magazine* 71: 347-363.

Wilkinson JJ (2001) Fluid inclusions in hydrothermal ore deposits. *Lithos* 55: 229-272.

Williams PJ (2010) Classifying IOCG deposits. In: Corriveau L, Mumin H (Eds) Exploring for iron-oxide copper-gold deposits: Canada and Global Analogues: *Geological Association.* Canada short course notes 20: 11–19.

Williams PJ, Barton MD, Johnson DA, Fontbote L, Haller AD, Mark G, Oliver NHS, Marschik R (2005) Iron oxide copper-gold deposits: geology, space-time distribution, and possible modes of origin. *Economic Geology* 100: 371-405.

Ziemann MA, Förster HJ, Harlov DE, Frei D (2005) Origin of fluorapatite-monazite assemblages in a metamorphosed, sillimanite-bearing pegmatoid, Reinbolt Hills, East Antartica. *European Journal of Mineralogy* 17: 567-579.